

Osteoarthritis and Cartilage (2006) 14, 1294–1301

© 2006 Osteoarthritis Research Society International. Published by Elsevier Ltd. All rights reserved.

doi:10.1016/j.joca.2006.05.012

Osteoarthritis and Cartilage

**International
Cartilage
Repair
Society**

Determination of *in-vivo* articular cartilage contact areas of human talocrural joint under weightbearing conditions

L. Wan B.S.^{†‡}, R. J. de Asla M.D.[†], H. E. Rubash M.D.[†] and G. Li Ph.D.^{†*}[†] *Bioengineering Laboratory, Department of Orthopaedic Surgery, Massachusetts General Hospital/Harvard Medical School, Boston, MA, USA*[‡] *Department of Physics, Massachusetts Institute of Technology, Cambridge, MA, USA*

Summary

Objective: The knowledge of *in-vivo* cartilage contact biomechanics is important to the understanding of the pathogenesis of joint diseases such as osteoarthritis. This study investigated the *in-vivo* contact areas of human talocrural joint under weightbearing conditions that *simulated* the stance phase of walking using a combined magnetic resonance (MR) and dual-orthogonal fluoroscopic imaging technique.

Design: Nine healthy ankles of living subjects were recruited for this study. The *in-vivo* talocrural joint positions were recorded using the dual-orthogonal fluoroscopic images at three ankle positions that simulated those occurring during the stance phase of walking: heel strike, mid-stance, and toe off. Three-dimensional (3D) models of the talocrural joints were created from MR images and used to reproduce the *in-vivo* ankle positions recorded on the fluoroscopic images. The talocrural cartilage contact area was defined as the overlap area of the distal tibial and the proximal talar cartilage surfaces. The method was validated using an *in-vitro* experimental setup to evaluate its accuracy in determination of cartilage contact area.

Results: The validation study demonstrated that the articular cartilage contact area of the talocrural joint determined using the imaging technique was approximately 4% lower than that of the experimental measurement. In the nine living ankles, the average cartilage coverage area was $964.9 \pm 156.1 \text{ mm}^2$ on the distal tibia and $1304.8 \pm 208.4 \text{ mm}^2$ on the proximal talus. The average talocrural cartilage contact areas were $272.7 \pm 61.1 \text{ mm}^2$ at heel strike, $416.8 \pm 51.7 \text{ mm}^2$ at mid-stance, and $335.7 \pm 64.5 \text{ mm}^2$ at toe off. The contact area at mid-stance was significantly larger than those at heel strike and toe off, while the contact area at toe off was significantly larger than that at heel strike.

Conclusion: The combined dual fluoroscopic and MR imaging technique was shown to be capable of determining *in-vivo* talocrural cartilage contact areas. During the simulated stance phase of walking, the contact areas were less than 44% and 31% of the cartilage coverage areas of the distal tibia and the proximal talus, respectively. These data may be useful for understanding *in-vivo* biomechanical function of the cartilage as well as the etiology of osteoarthritis.

© 2006 Osteoarthritis Research Society International. Published by Elsevier Ltd. All rights reserved.

Key words: Cartilage, Cartilage contact, *In-vivo* biomechanics, Ankle joint, Talocrural joint.

Introduction

The talocrural (ankle) joint is an important weightbearing articulation in the human body. Ground reaction forces transmitted through the talocrural joint were reported to be two to three times the body weight during gait^{1,2}. However, very few studies have reported on *in-vivo* articular cartilage contact behavior of the talocrural joint. This knowledge is critical for understanding the pathogenesis of joint diseases such as osteoarthritis and for the design of ankle joint arthroplasties since abnormal contact mechanics is generally believed to cause osteoarthritis³.

Talocrural joint contact has been studied mostly using *in-vitro* cadaveric ankle specimens^{4–17}. For example, Ramsey and Hamilton⁴ used carbon black transference techniques to determine the contact area in the tibiotalar articulations with the talus in its neutral position and displaced

laterally. Others used pressure sensors or pressure-sensitive film to determine the contact areas and pressure distributions on the proximal talar surface under various simulated talocrural conditions^{5–15}. Kinematic tracking methods have also been used to determine ankle joint contact area^{16,17}, such as the magnetic tracking device combined with proximity calculations of digitized joint surfaces used by Kura *et al.*¹⁶, the radiostereometric analysis (RSA) combined with three-dimensional (3D) surface modeling used by Corazza *et al.*¹⁷. Despite these various *in-vitro* investigations, measurement of *in-vivo* cartilage contact areas of the talocrural joint under functional loading conditions remains a challenge in biomedical engineering.

Recently, a novel technique using dual-orthogonal fluoroscopic images and magnetic resonance (MR) image-based computer models was introduced to study *in-vivo* articular cartilage contact kinematics of the knee^{18–20}. In this paper, this method was adapted to study the *in-vivo* articular cartilage contact patterns of the talocrural joint on both the distal tibia and proximal talus at three weightbearing positions that simulated three positions of the stance phase of walking. MR image-based talocrural joint models were used to reproduce the 6 degrees-of-freedom (DOF) *in-vivo* ankle positions. Cartilage-to-cartilage contact area was

*Address correspondence and reprint requests to: G. Li, Ph.D., Bioengineering Laboratory, Department of Orthopaedic Surgery, Massachusetts General Hospital/Harvard Medical School, 55 Fruit Street, GRJ 1215, Boston, MA 02114, USA. Tel: 1-617-726-6472; Fax: 1-617-724-4392; E-mail: gli1@partners.org

Received 12 January 2006; revision accepted 13 May 2006.

then determined by quantifying the amount of overlap of the cartilage surfaces of the tibia and talus. The methodology used to measure talocrural cartilage contact area was validated using an *in-vitro* experimental setup.

Materials and method

Nine normal ankles from seven healthy volunteers (three males and four females, 24–45 years old) were recruited with the approval of our institutional review board (IRB). The averaged body weight of the volunteers was 67.4 ± 13.1 kg and the averaged height was 169.3 ± 10.3 cm. The averaged body mass index (BMI) was 23.9 ± 4.4 . Two male volunteers had both of their ankles studied while others had only one. Four ankles were left and five were right. The ankles had no history of injuries and no signs of osteoarthritis.

MR IMAGING AND 3D MODEL

Each ankle recruited for this study was MR imaged on a 1.5-T magnet (GE, Milwaukee, WI) using a surface coil and three-dimensional spoiled gradient-recalled (3D SPGR) sequence with the subject lying supine (TR = 48 ms, TE = 4.3 ms, Flip Angle = 45° , FOV = 16×16 cm²). A cubic volume ($16 \times 16 \times 10$ cm³) enclosing the talocrural joint was MR scanned with 16 cm in both anterior–posterior and proximal–distal directions [Fig. 1(a)] and 10 cm in medial–lateral direction. Parallel sagittal images with a resolution of 512×512 pixels were separated at 1 mm intervals. For each ankle, the scan time was approximately 11 min. The MR images were imported into a solid modeling software package (Rhinoceros®, Seattle, WA) for digitization of the outlines of the tibia, talus and their cartilage surfaces. The digitized spatial data (x, y, z coordinates) were then linked using B-spline curves to reproduce the contours of the tibia and talus. Bone and cartilage surfaces of the tibia and talus were created from the contours using polygon mesh. This method has been used extensively in previous publication²¹. A typical talocrural joint model constructed from MR images is shown in Fig. 1(b).

DUAL-ORTHOGONAL FLUOROSCOPIC SYSTEM

A dual-orthogonal fluoroscopic imaging system was used to measure *in-vivo* ankle joint kinematics²². In this system, two fluoroscopes (OEC® 9800 ESP, GE, Salt Lake City)

were positioned in such a way that the two image intensifiers were perpendicular to each other in the horizontal plane²³. During the experiment, the subject walked on a platform and once the ankle was in front of the two image intensifiers, the ankle positions were recorded simultaneously from anteromedial and anterolateral directions by the two fluoroscopes (Fig. 2). The resolution of the images collected from the fluoroscopes was 1000×1000 pixels. Various ankle positions during functional activities can be recorded using this system. In this study, each subject was instructed to reproduce three ankle positions representative during the stance phase of level walking: heel strike (at the early phase of walking, the heel of the target foot touches the ground and carries partial body weight), mid-stance (at the middle phase of walking, the target foot carries full body weight), and toe off (at the late phase of walking, only the toes of the target foot touch the ground and carry partial body weight). At each of these positions, the ankle was held still for 1 s for the two fluoroscopes to capture the ankle position.

DETERMINATION OF *IN-VIVO* CARTILAGE CONTACT AREA

To determine *in-vivo* talocrural joint kinematics, the 3D talocrural joint model and the orthogonal fluoroscopic images were imported into the solid modeling software to create a virtual dual-orthogonal fluoroscopic system²². Two virtual cameras were created to reproduce the positions of the X-ray sources of the two fluoroscopes during the imaging acquisition. The orthogonal images were placed as two virtual image intensifiers [Fig. 3(a)]. The 3D talocrural joint model was then imported into the virtual space. The virtual cameras projected the joint model onto the corresponding virtual image intensifiers [Fig. 3(a)]. The positions of the tibial and talus models were manually adjusted individually in 6 DOF until their projections matched the contours of the actual talocrural joint on the two fluoroscopic images [Fig. 3(a)]. The 3D talocrural joint model then reproduced the *in-vivo* ankle position recorded on the dual fluoroscopic images [Fig. 3(b)].

Once the talocrural joint positions were determined, the relative positions of the cartilage surfaces of the tibia and talus were determined. At each ankle position reproduced in the virtual space, the tibial and talar cartilage surfaces (of the ankle model) showed partial overlap. In this study, this overlap was assumed to indicate the locations where

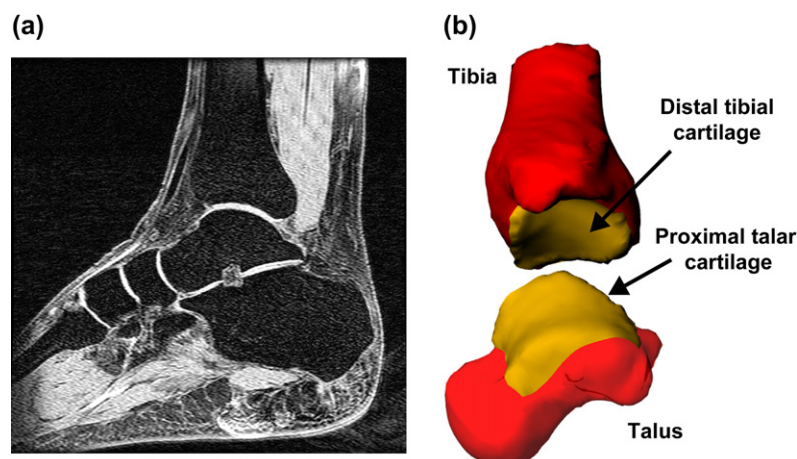


Fig. 1. (a) A typical sagittal plane MR image of the talocrural joint; (b) 3D bony and cartilage model of the talocrural joint.

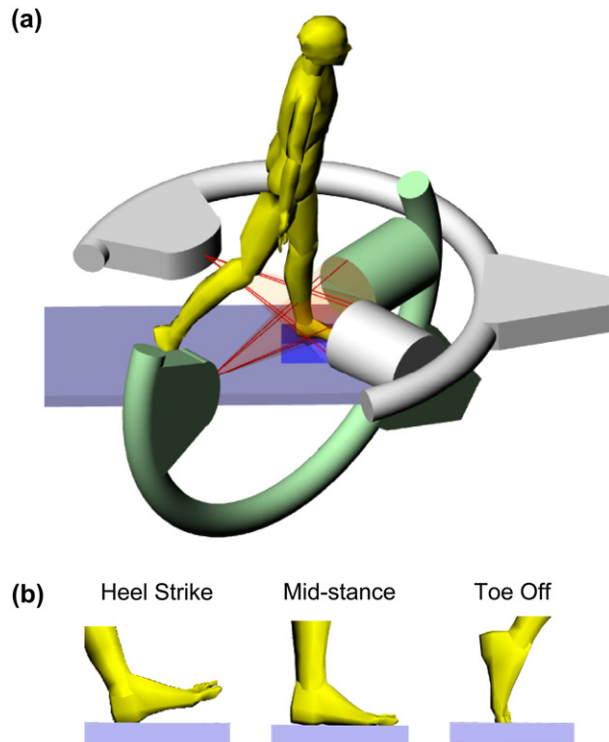


Fig. 2. (a) The dual-orthogonal fluoroscopic system setup for measurement of *in-vivo* ankle joint kinematics; (b) three weightbearing positions of the foot captured in this study.

the articular surfaces were in contact. The area was determined by identifying the intersection of the cartilage surfaces, with the use of the solid modeling software.

To study the contact patterns at the talocrural joint, both tibial and talar surfaces were evenly divided into nine sub-regions [Fig. 4(a) and (b)]. Each sub-region was labeled by two letters in vertical and horizontal directions, respectively. Similar to the contact frequency as defined in previously published data on ankle and shoulder joints^{16,24}, we defined a modified contact frequency to describe the contact patterns at the talocrural joint in this paper as the percentage of the contact area at a sub-region with respect to the overall contact.

SYSTEM VALIDATION

A validation was performed to assess the accuracy of the combined MR and fluoroscopic imaging technique when used to measure cartilage contact areas of the talocrural joint. A human cadaveric foot specimen (male, 68 years old) with a 40 cm tibia shaft was MR imaged and a 3D anatomic talocrural joint model was constructed, including the bony surfaces of the tibia and talus, as well as the corresponding cartilage surfaces.

After the MR imaging scan, the talocrural joint was separated at the talocrural joint line and installed on a robotic testing system²⁵. In this setup, the foot of the specimen was rigidly fixed on a pedestal while the tibia was fixed to the robot through a 6 DOF load cell. The talus was left on the foot and not fixed using additional constraints. The robot could apply a load to the tibia, causing talocrural joint compression. In this validation study, the ankle was loaded along the tibial axis to about 200 N. The robot recorded the ankle position under the load. The talocrural joint was

then separated and liquid silicone rubber²⁶ was placed between the tibia and the talus. The tibia was returned to the position measured by the robot under the 200 N axial load. The silicone rubber was squeezed away from the area of articular cartilage contact and was kept in that position for 1 min until the rubber hardened. The talocrural joint was then imaged using the dual-orthogonal fluoroscopic image system. The ankle was separated immediately to digitize the contact area. The entire procedure took less than 5 min. The ankle joint was sprayed regularly with saline to keep the joint from dehydrating. The cartilage contact area was represented by a hole in the silicone rubber [Fig. 5(a)], which was digitized using a stylus (Microscribe 3DX[®], Immersion Technologies, San Jose, CA). In addition, anatomic landmarks on the tibia and talus were also digitized so that the contact area measured from the silicone casting method could be aligned with the 3D talocrural model. The actual contact area could be compared to that obtained from the image matching method.

The pair of fluoroscopic images of the ankle captured when the ankle joint was under compression and the 3D models of the tibia and talus were used to reproduce the ankle position in the virtual fluoroscopic system using the same procedures as for the *in-vivo* study mentioned before. The ankle position under load was matched five times independently in this validation study to evaluate the repeatability of the matching process in determination of cartilage contact area. The cartilage contact area determined in this fashion was then compared with that measured from the silicone casting method, which represented a rigorous validation of the contact area obtained using the combined MR and dual-orthogonal fluoroscopic imaging technique.

DATA ANALYSIS

In this paper, we first presented the data that validated the accuracy of the image matching method in determination of the articular cartilage contact area. We then presented the cartilage contact areas of the talocrural joint at various weightbearing conditions, i.e., *simulated* heel strike, mid-stance and toe off positions. The cartilage contact frequencies on both the tibial and talar surfaces were calculated to describe cartilage contact patterns. A repeated measure ANOVA was used to compare the cartilage contact areas between different foot positions. The statistically significant difference was defined as $P < 0.05$.

Results

SYSTEM VALIDATION

In the *in-vitro* validation study, the cartilage contact area at the talocrural joint measured using the silicone casting method was 579.1 mm² under a 200 N compressive load [Fig. 5(a)]. The contact area measures obtained from the five independent image matching processes averaged 568.9 ± 22.2 mm² [Fig. 5(b)]. The coefficient of variance (the ratio of the standard deviation to the mean value, as a percentage) was 3.9%. This area measurement (by the image method) was approximately 3.4% smaller than the physical measurement by the silicone casting method (579.1 mm²).

IN-VIVO CARTILAGE CONTACT AREA AT TALOCRURAL JOINT

Cartilage coverage areas of each talocrural joint were calculated. The average cartilage coverage area of the nine

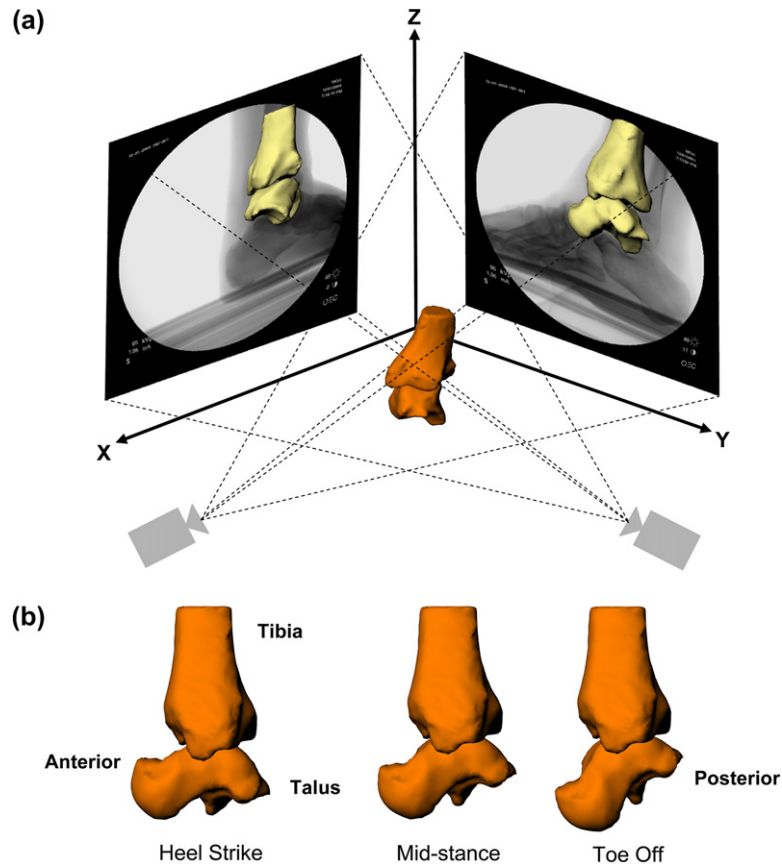


Fig. 3. (a) The virtual dual fluoroscopic system used to reproduce the *in-vivo* talocrural position; (b) medial view of the talocrural joint during the stance phase of walking (cartilage not shown) reproduced using the virtual dual fluoroscopic system.

ankles was $964.9 \pm 156.1 \text{ mm}^2$ on the tibial surface and $1304.8 \pm 208.4 \text{ mm}^2$ on the talar surface.

The cartilage contact areas of a typical talocrural joint during the simulated stance phase of walking are illustrated in Fig. 6. At heel strike position, the average contact area of the nine ankles was $272.7 \pm 61.1 \text{ mm}^2$ (Fig. 7), which accounted for $28.2 \pm 4.2\%$ of the tibial cartilage surface area and $20.9 \pm 3.6\%$ of the talar cartilage surface area. At mid-stance position, the cartilage contact area was $416.8 \pm 51.7 \text{ mm}^2$, which accounted for $43.7 \pm 5.5\%$ of the tibial cartilage surface area and $31.0 \pm 5.0\%$ of the talar cartilage surface area. At toe off position, the cartilage contact area was $335.7 \pm 64.5 \text{ mm}^2$, which accounted for $34.8 \pm 4.1\%$ of the tibial cartilage surface area and $25.8 \pm 3.9\%$ of the talar cartilage surface area. The contact area at simulated mid-stance was significantly larger than those at simulated heel strike ($P=0.0001$) and toe off ($P=0.0004$), while the contact area at simulated heel strike was significantly smaller than that at simulated toe off ($P=0.0028$) (Fig. 7).

IN-VIVO CARTILAGE CONTACT PATTERNS AT TALOCRURAL JOINT

Cartilage contact frequencies of the talocrural joint at different foot positions during the simulated stance phase of walking are shown in Table I. The average flexion angles of the talocrural joint were calculated using the same protocol as in our previous work²². From heel strike to

mid-stance, the talocrural joint plantarflexed $4.9 \pm 8.1^\circ$ in these nine subjects. From mid-stance to toe off, the talocrural joint only plantarflexed $0.2 \pm 12.5^\circ$. At the simulated heel strike position, the highest contact frequency on the tibial surface was observed at the lateral–central sub-region ($18.9 \pm 13.4\%$) and lowest at the medial–posterior sub-region ($3.5 \pm 9.6\%$). On the talar surface, the highest contact frequency was also measured at the lateral–central sub-region ($22.1 \pm 15.0\%$) and the lowest was at the medial–posterior sub-region ($0.6 \pm 1.7\%$). At the simulated mid-stance position, the highest contact frequency was observed at the lateral–central sub-region ($21.4 \pm 3.9\%$) and the lowest was at the medial–posterior sub-region ($1.4 \pm 3.7\%$) of the tibial surface. On the talar surface, the highest contact frequency was found also at the lateral–central sub-region ($24.5 \pm 7.8\%$) and lowest at the medial–posterior sub-region ($1.4 \pm 2.5\%$). At the simulated toe off position, the highest contact frequency was measured at the central–central sub-region of the tibial surface ($18.5 \pm 7.1\%$) and the lowest was at the lateral–posterior sub-region ($1.7 \pm 1.9\%$). On the talar surface, the highest contact frequency was also at the central–central sub-region ($17.8 \pm 11.9\%$) and the lowest was at the lateral–posterior sub-region ($5.5 \pm 5.6\%$).

Discussion

This study investigated the *in-vivo* articular cartilage contact area at the talocrural joint under weightbearing

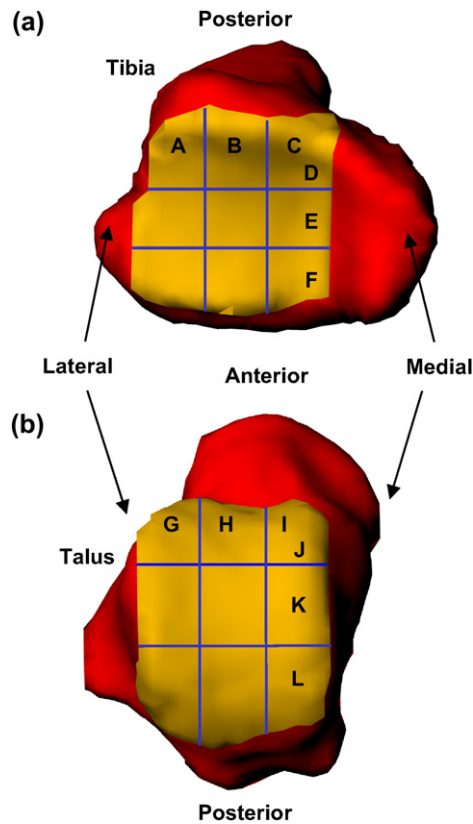


Fig. 4. (a) Nine sub-regions of the distal tibial cartilage surface; (b) nine sub-regions of the proximal talar cartilage surface. The nine sub-regions are identified by the letters on both the tibial and talar cartilage surfaces.

conditions that simulated the stance phase of walking using a combined MR and dual-orthogonal fluoroscopic imaging technique. Our validation demonstrated that the cartilage contact area at the talocrural joint could be accurately determined using this imaging technique.

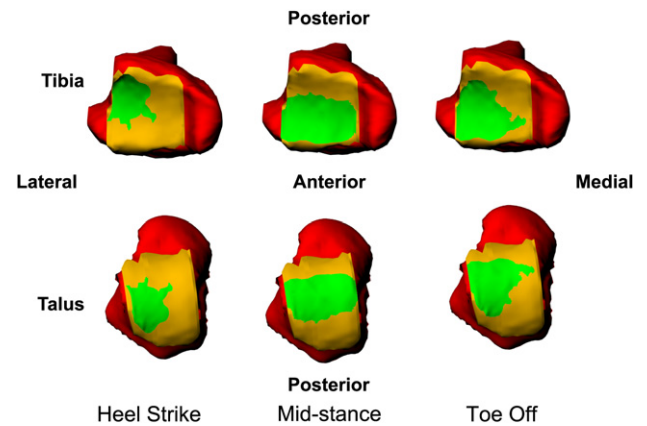


Fig. 6. *In-vivo* cartilage contact patterns during the simulated stance phase of walking of a typical talocrural joint.

Coverage areas of cartilage surfaces of the talocrural joint have been reported in several studies^{7,16,27,28}. Data from these studies are shown in Table II. Although there is no unique standard on definition of the boundaries of cartilage coverage areas of the distal tibial surface and the proximal talar surface, all these data were similar with ours, where a $964.9 \pm 156.1 \text{ mm}^2$ was measured for the tibial cartilage surface and $1304.8 \pm 208.4 \text{ mm}^2$ for the talar cartilage surface.

Cadaveric experimental setups have been used in various studies to estimate cartilage contact areas at the talocrural joint^{4,7,9,29}. Most of these experiments used pressure sensors or pressure-sensitive film. Kimizuka *et al.*²⁹ measured average *in-vitro* talocrural contact areas of 434 mm^2 and 484 mm^2 under 1000 N and 1500 N compressive loads, respectively. Driscoll *et al.*⁹ measured a total contact area of $327.4 \pm 31.9 \text{ mm}^2$ under a compressive load of 800 N with 10% of the load applied through the fibula. Ramsey and Hamilton⁴ reported a contact area of $440 \pm 121 \text{ mm}^2$ under a compressive load of 700 N . Under a 500 N loading, Kimizuka *et al.*²⁹ measured

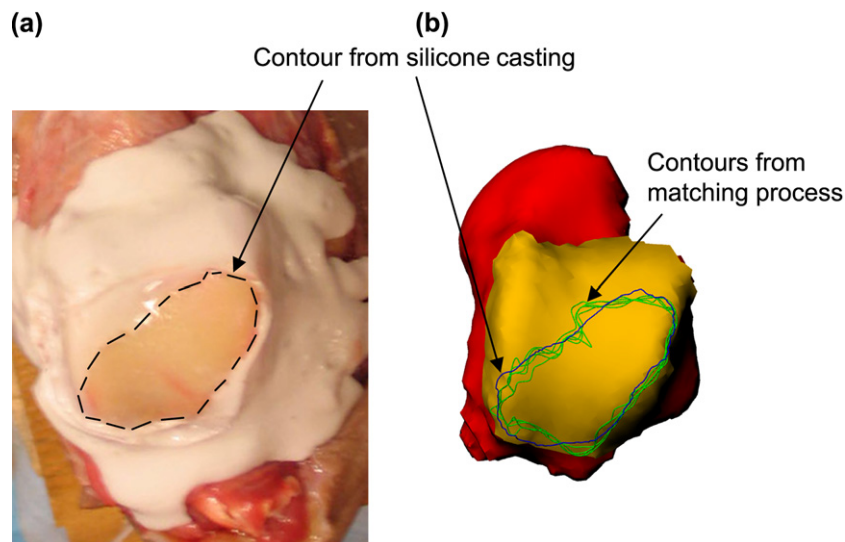


Fig. 5. (a) The contact pattern measured using silicone casting method in a cadaveric foot specimen; (b) 3D talus model with blue contour representing the contact pattern from silicone casting method and green contours representing the contact patterns obtained from five image matching processes.

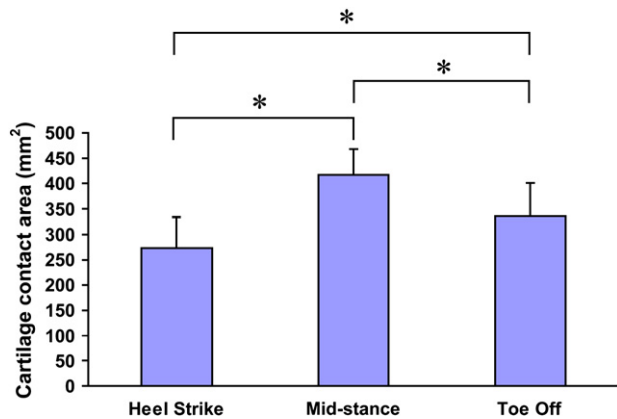


Fig. 7. Talocrural cartilage contact areas during the simulated stance phase of walking (* $P < 0.05$).

a contact area of 343 mm² in the talocrural joint while Bruns and Rosenbach⁷ measured a contact area of 155.1 ± 60.3 mm² under the same load later. Our data indicated that under weightbearing conditions that simulated the stance phase of walking, the mean cartilage contact area of the talocrural joint was between 272 mm² and 417 mm². All these various studies demonstrated that the cartilage contact areas were less than 500 mm² at the talocrural joint.

The results of our study indicated that articular cartilage contact was only observed in less than 50% of the cartilage coverage areas in the talocrural joint at various positions of the simulated stance phase of walking. Since the exact *in-vivo* loading condition at the talocrural joint is unknown,

Table I

(a) The modified contact frequencies (%) at the sub-regions of tibial cartilage surface corresponding to Fig. 4(a) at different positions of the simulated stance phase of walking; (b) the modified contact frequencies (%) at the sub-regions of talar cartilage surface corresponding to Fig. 4(b) at different positions of the simulated stance phase of walking

(a)			
	A	B	C
Heel strike	9.3 ± 10.3	13.8 ± 12.8	3.5 ± 9.6
Mid-stance	4.4 ± 4.3	10.0 ± 11.5	1.4 ± 3.7
Toe off	1.7 ± 1.9	10.6 ± 10.5	6.1 ± 9.1
Heel strike	18.9 ± 13.4	11.4 ± 7.5	7.7 ± 13.4
Mid-stance	21.4 ± 3.9	20.0 ± 5.6	5.1 ± 4.6
Toe off	15.9 ± 10.9	18.5 ± 7.1	8.3 ± 7.7
Heel strike	10.0 ± 9.2	17.8 ± 15.3	7.6 ± 6.9
Mid-stance	13.8 ± 6.9	15.5 ± 6.4	8.4 ± 7.1
Toe off	13.2 ± 8.5	18.2 ± 10.5	7.5 ± 5.7
(b)			
	G	H	I
Heel strike	9.6 ± 0.4	17.1 ± 19.1	7.6 ± 9.6
Mid-stance	7.8 ± 5.5	10.9 ± 8.8	5.8 ± 6.7
Toe off	10.8 ± 12.8	13.7 ± 16.1	5.9 ± 7.3
Heel strike	22.1 ± 15.0	13.3 ± 11.5	11.4 ± 22.2
Mid-stance	24.5 ± 7.8	22.6 ± 4.9	9.8 ± 8.1
Toe off	16.2 ± 12.8	17.8 ± 11.9	9.7 ± 13.5
Heel strike	8.0 ± 7.9	10.3 ± 11.7	0.6 ± 1.7
Mid-stance	5.7 ± 4.7	11.4 ± 12.7	1.4 ± 2.5
Toe off	5.5 ± 5.6	12.6 ± 16.0	7.8 ± 12.6

Table II
Cartilage coverage areas on the distal tibial surface and proximal talar surface reported in literature

	Tibial cartilage area (mm ²)	Talar cartilage area (mm ²)
Bruns and Rosenbach ⁷	N/A	1196.7 ± 190.4
Kura <i>et al.</i> ¹⁶	922 ± 120	N/A
Al-Ali <i>et al.</i> ²⁷	1020 ± 188	1390 ± 274
Greenwald <i>et al.</i> ²⁸	N/A	1329.0 ± 167.7

it is difficult to compare our data with those reported in the literature. Our *in-vivo* cartilage contact data showed significant changes in cartilage contact areas at different positions that simulated those during the stance phase of walking (Fig. 7). This might be indicative of the effect of the varying loading conditions throughout the simulated stance phase of walking as well as the complicated geometry of the joint. The cartilage of the talocrural joint was only partially loaded during the various *in-vivo* loading conditions.

Contact frequency has been used in literature to represent the locations of cartilage contact in articular joints such as the ankle¹⁶ and the shoulder²⁴. In this study, we divided the cartilage surfaces of the talocrural joint into nine sub-regions. The percentage of the contact area in a sub-region was defined as the contact frequency in the sub-region. In the three ankle positions studied in this paper, the highest contact frequency was less than 25%, indicating no dominance of the contact locations was found. The lowest contact frequencies were always found at the posterior regions on both the tibial and talar surfaces. In general, the contact areas were found to be slightly more lateral and central at heel strike and mid-stance positions (Fig. 4). This contact pattern might correlate to the ankle kinematics during the gait. Eversion (valgus) positioned hind feet were generally observed from heel strike to mid-stance during the stance phase of walking^{22,30,31}. As reported in our previous work about the 6 DOF kinematics of human ankle joint complex²², the motion of the joint at these positions was not simply dorsi-plantar flexion, inversion-eversion or internal-external rotation, but rather a coupled motion. Small joint position changes may cause significant changes of contact area. Our data indicated that an eversion ankle position might shift the *in-vivo* talocrural joint contact more laterally, which has also been observed in previous cadaveric experiments^{22,30,31}. From mid-stance to toe off positions, the most frequent contact region slightly shifted to more central. This might be caused by the reduced eversion of the ankle during this motion as stated in other literature⁸.

There are several limitations that should be noted in this study. We used overlap of two cartilage surfaces to represent the cartilage contact area. This might underestimate the contact area since the cartilage deforms under load. Deformation of the cartilage might result in larger contact area than the overlapping area. This method was only validated under a static loading condition. The validation test indicated that the image matching method caused a 3.4% underestimate in the contact area under a 200 N load. Therefore, the image matching method could provide a useful estimation of the *in-vivo* talocrural cartilage contact areas.

The contact stress distributions in the cartilage layers were not obtained in this study. However, the contact kinematics of the talocrural joint determined from this study may be used as a displacement boundary condition for a 3D

finite element analysis to calculate the actual cartilage contact areas and stress distributions within the talocrural joint. To do this, the constitutive behavior of the *in-vivo* cartilage must be known *a priori*, which makes the *in-vivo* finite element analysis challenging. Another limitation of this study is that we only investigated three positions during the simulated stance phase of walking and none of these positions were captured in real time during walking²². It is known that the cartilage deformation is time-dependent. Cartilage contact behavior may need to be described as a function of loading history of the functional activity. Future study will investigate the talocrural cartilage contact areas and stress distributions during the real dynamic stance phase of walking using cine-fluoroscopy.

In conclusion, the combined MR and dual-orthogonal fluoroscopic imaging method was shown to be a valuable tool for the determination of the *in-vivo* articular cartilage contact areas of the talocrural joint at various weightbearing ankle positions. At the positions that simulated the stance phase of walking, the contact area was less than half of the cartilage coverage areas of the tibial and talar surfaces. The contact areas were shown to be slightly more lateral and central on the talocrural joint surfaces; and in general, the posterior portion of the talocrural joint showed lower contact frequencies as compared with other regions. These quantitative data may be useful for the development of 3D finite element modeling of *in-vivo* cartilage contact stress. This methodology can also be used to investigate the contact biomechanics of ankle joints with osteoarthritis.

Acknowledgment

This study was partially supported by the Department of Orthopaedic Surgery of Massachusetts General Hospital and National Institute of Health (AR052408). We also thank Ramprasad Papannagari, Louis E DeFrate, Jeremy F Suggs, Jeffrey T Bingham, George R Hanson, Daniel F Massimini, and Samuel Van de Velde for their technical assistance.

References

- Procter P, Paul JP. Ankle joint biomechanics. *J Biomech* 1982;15:627–34.
- Nuber GW. Biomechanics of the foot and ankle during gait. *Clin Sports Med* 1988;7:1–13.
- Llinas A, McKellop HA, Marshall GJ, Sharpe F, Kirchen M, Sarmiento A. Healing and remodeling of articular incongruities in a rabbit fracture model. *J Bone Joint Surg Am* 1993;75:1508–23.
- Ramsey PL, Hamilton W. Changes in tibiotalar area of contact caused by lateral talar shift. *J Bone Joint Surg Am* 1976;58:356–7.
- Steffensmeier SJ, Saltzman CL, Berbaum KS, Brown TD. Effects of medial and lateral displacement calcaneal osteotomies on tibiotalar joint contact stresses. *J Orthop Res* 1996;14:980–5.
- Michelson JD, Checcone M, Kuhn T, Varner K. Intra-articular load distribution in the human ankle joint during motion. *Foot Ankle Int* 2001;22:226–33.
- Bruns J, Rosenbach B. Pressure distribution at the ankle joint. *Clin Biomech* 1990;5:153–61.
- Calhoun JH, Li F, Ledbetter BR, Viegas SF. A comprehensive study of pressure distribution in the ankle joint with inversion and eversion. *Foot Ankle Int* 1994;15:125–33.
- Driscoll HL, Christensen JC, Tencer AF. Contact characteristics of the ankle joint. Part 1. The normal joint. *J Am Podiatr Med Assoc* 1994;84:491–8.
- Christensen JC, Driscoll HL, Tencer AF. Contact characteristics of the ankle joint. Part 2. The effects of talar dome cartilage defects. *J Am Podiatr Med Assoc* 1994;84:537–47.
- Tarr RR, Resnick CT, Wagner KS, Sarmiento A. Changes in tibiotalar joint contact areas following experimentally induced tibial angular deformities. *Clin Orthop* 1985;199:72–80.
- Ting AJ, Tarr RR, Sarmiento A, Wagner K, Resnick C. The role of subtalar motion and ankle contact pressure changes from angular deformities of the tibia. *Foot Ankle* 1987;7:290–9.
- Beaudoin AJ, Fiore SM, Krause WR, Adelaar RS. Effect of isolated talocalcaneal fusion on contact in the ankle and talonavicular joints. *Foot Ankle* 1991;12:19–25.
- Pereira DS, Koval KJ, Resnick RB, Sheslier SC, Kummer F, Zuckerman JD. Tibiotalar contact area and pressure distribution: the effect of mortise widening and syndesmosis fixation. *Foot Ankle Int* 1996;17:269–74.
- Wagner KS, Tarr RR, Resnick C, Sarmiento A. The effect of simulated tibial deformities on the ankle joint during the gait cycle. *Foot Ankle* 1984;5:131–41.
- Kura H, Kitaoka HB, Luo ZP, An KN. Measurement of surface contact area of the ankle joint. *Clin Biomech (Bristol, Avon)* 1998;13:365–70.
- Corazza F, Stagni R, Parenti Castelli V, Leardini A. Articular contact at the tibiotalar joint in passive flexion. *J Biomech* 2005;38:1205–12.
- DeFrate LE, Sun H, Gill TJ, Rubash HE, Li G. *In vivo* tibiofemoral contact analysis using 3D MRI-based knee models. *J Biomech* 2004;37:1499–504.
- Li G, DeFrate LE, Park SE, Gill TJ, Rubash HE. *In vivo* articular cartilage contact kinematics of the knee: an investigation using dual-orthogonal fluoroscopy and magnetic resonance image-based computer models. *Am J Sports Med* 2005;33:102–7.
- Li G, Wuerz TH, DeFrate LE. Feasibility of using orthogonal fluoroscopic images to measure *in vivo* joint kinematics. *J Biomech Eng* 2004;126:314–8.
- Li G, Lopez O, Rubash H. Variability of a three-dimensional finite element model constructed using magnetic resonance images of a knee for joint contact stress analysis. *J Biomech Eng* 2001;123:341–6.
- de Asla RJ, Wan L, Rubash HE, Li G. 6 DOF *In-vivo* kinematics of the ankle joint complex – application of a combined dual-orthogonal fluoroscopic and MR imaging technique. *J Orthop Res* 2006;24:1019–27.
- Hanson GR, Suggs JF, Freiberg AA, Durbhakula SD, Rubash HE, Li G. Investigate of *in vivo* 6DOF TKA kinematics using a dual orthogonal fluoroscopic system. *J Orthop Res* 2006;24:974–81.
- Soslowsky LJ, Flatow EL, Bigliani LU, Pawluk RJ, Ateshian GA, Mow VC. Quantitation of *in situ* contact areas at the glenohumeral joint: a biomechanical study. *J Orthop Res* 1992;10:524–34.
- Li G, Most E, Sultan PG, Schule S, Zayontz S, Park SE, *et al.* Knee kinematics with a high-flexion posterior stabilized total knee prosthesis: an *in vitro* robotic experimental investigation. *J Bone Joint Surg Am* 2004;86-A:1721–9.

-
26. Stormont TJ, An KN, Morrey BF, Chao EY. Elbow joint contact study: comparison of techniques. *J Biomech* 1985;18:329–36.
 27. Al-Ali D, Graichen H, Faber S, Englmeier KH, Reiser M, Eckstein F. Quantitative cartilage imaging of the human hind foot: precision and inter-subject variability. *J Orthop Res* 2002;20:249–56.
 28. Greenwald AS, Matejczyk MB, Keppler L, Black JD Jr, Moran JM, Porritt D, *et al.* Preliminary observations on the weight-bearing surfaces of the human ankle joint. *Surg Forum* 1976;27:505–6.
 29. Kimizuka M, Kurosawa H, Fukubayashi T. Load-bearing pattern of the ankle joint. Contact area and pressure distribution. *Arch Orthop Trauma Surg* 1980;96:45–9.
 30. Moseley L, Smith R, Hunt A, Gant R. Three-dimensional kinematics of the rearfoot during the stance phase of walking in normal young adult males. *Clin Biomech (Bristol, Avon)* 1996;11:39–45.
 31. Arndt A, Westblad P, Winson I, Hashimoto T, Lundberg A. Ankle and subtalar kinematics measured with intracortical pins during the stance phase of walking. *Foot Ankle Int* 2004;25:357–64.
-